Identification of Small Molecule Inhibitors of the Deubiquitinating Activity of the SARS-CoV-2 Papain-Like Protease: *in silico* Molecular Docking Studies and *in vitro* Enzymatic Activity Assay

Eleni Pitsillou [1,2], Julia Liang [1,2], Katherine Ververis [1], Kah Wai Lim [1,3], Andrew Hung [2] and Tom C. Karagiannis [1,4]*

[1] Epigenomic Medicine, Department of Diabetes, Central Clinical School, Monash University, Melbourne, VIC, Australia, [2] School of Science, College of Science, Engineering and Health, RMIT University, Melbourne, VIC, Australia, [3] Department of Microbiology and Immunology, The University of Melbourne, Parkville, VIC, Australia, [4] Department of Clinical Pathology, The University of Melbourne, Parkville, VIC, Australia

COVID-19 is an ongoing pandemic caused by the SARS-CoV-2 virus with important political, socio-economic, and public health consequences. Inhibiting replication represents an important antiviral approach, and in this context two viral proteases, the SARS-CoV-2 main and papain-like proteases (PL^{pro}), which cleave pp1a and pp1ab polypeptides, are critical. Along with protease activity, the PL^{pro} possesses deubiquitinating activity, which is important in immune regulation. Naphthalene-based inhibitors, such as the well-investigated GRL-0617 compound, have been shown to possess dual effects, inhibiting both protease and deubiquitinating activity of the PL^{pro}. Rather than binding to the canonical catalytic triad, these type of non-covalent inhibitors target an adjacent pocket, the naphthalene-inhibitor binding site. Using a high-throughput screen, we have previously identified the dietary hypericin, rutin, and cyanidin-3-O-glucoside compounds as potential protease inhibitors targeting the naphthalene-inhibitor binding site. Here, our aim was to investigate the binding characteristics of these compounds to the PL^{pro}, and to evaluate deubiquitinating activity, by analyzing seven different PL^{pro} crystal structures. Molecular docking highlighted the relatively high affinity of GRL-0617 and dietary compounds. In contrast binding of the small molecules was abolished in the presence of ubiquitin in the palm subdomain of the PL^{pro}. Further, docking the small molecules in the naphthalene-inhibitor binding site, followed by protein-protein docking revealed displacement of ubiquitin in a conformation inconsistent with functional activity. Finally, the deubiquitinating activity was validated *in vitro* using an enzymatic activity assay. The findings indicated that the dietary compounds inhibited deubiquitinase activity in the micromolar range with an order of activity of GRL-0167, hypericin >> rutin, cyanidin-3-O-glucoside > epigallocatechin gallate, epicatechin gallate, and cefotaxime. Our findings are in accordance with

mechanisms and potential antiviral effects of the naphthalene-based, GRL-0617 inhibitor, which is currently progressing in preclinical trials. Further, our findings indicate that in particular hypericin, rutin, and cyanidin-3-O-glucoside, represent suitable candidates for subsequent evaluation as PL^{pro} inhibitors.

INTRODUCTION

Coronavirus disease (COVID-19) was declared a pandemic on the 11th of March 2020 (World Health Organization, 2020). The first reported cases of this disease came from Wuhan, China in late 2019, and the infectious agent responsible for causing this disease was identified as severe acute respiratory syndrome coronavirus 2 (SARS-CoV-2) (Coronaviridae Study Group of the International Committee on Taxonomy of Viruses, 2020). Since the start of the year, the scientific literature on COVID-19 has increased and the findings from these studies have formed an integral part of the public health response.

In regards to treatment options, a number of vaccine trials have been established and there is also a focus on drug repositioning (Bar-Zeev and Moss, 2020; Folegatti et al., 2020). The U.S Food and Drug Administration (FDA) has recently approved remdesivir, which is an RNA-dependent RNA polymerase inhibitor, as a COVID-19 treatment for hospitalized patients (FDA, 2020). Interestingly, the WHO Solidarity trial has produced contradicting findings regarding the effectiveness of remdesivir (Pan H. et al., 2020). In addition to antiviral drugs, the efficacy of compounds that have immunomodulating properties are also being investigated (de la Rica et al., 2020).

Further research is required to establish the precise mechanisms of action of potential therapeutic drugs and determine their biological targets (Zhou Y. et al., 2020). The virus replication cycle is comprised of several stages and compounds that inhibit key proteins involved in these steps may have antiviral properties (Jeong et al., 2020; Pandey et al., 2020). Papain-like protease (PL^{pro}) is a cysteine protease enzyme that is encoded by the multi-domain non-structural protein 3 (nsp3) and is required for polypeptide processing (Báez-Santos et al., 2015; Folegatti et al., 2020). The role of the SARS-CoV-2 PL^{pro} in viral replication and the regulation of the innate immune response is being explored (Shin et al., 2020).

Ubiquitin and ubiquitin-like proteins, such as interferon-stimulated gene 15 (ISG15), are important effector molecules of the antiviral immune response (Jiang and Chen, 2011; Perng and Lenschow, 2018). Through binding to target proteins, various cellular pathways can be modulated (Jiang and Chen, 2011; Perng and Lenschow, 2018). Viruses have developed mechanisms to evade detection and destruction by the host's immune response, and these strategies continue to evolve (Nelemans and Kikkert, 2019). In terms of SARS-CoV-2, the deubiquitinating and deISGylating activities of the PL^{pro} enzyme have been described (Bosken et al., 2020; Klemm et al., 2020; Rut et al., 2020; Shin et al., 2020). GRL-0617 is a naphthalene-based inhibitor that has

been found to interfere with the protease, deubiquitinase and deISGylating activities of the SARS-CoV and SARS-CoV-2 PL^{pro} enzymes (Ratia et al., 2008; Freitas et al., 2020; Gao et al., in press). The SARS-CoV-2 PL^{pro} has consequently been identified as an attractive drug target and in this study, the deubiquitinase activity of this viral protein was of interest (McClain and Vabret, 2020).

The health-promoting properties of dietary compounds have been extensively explored over the years and in response to the COVID-19 pandemic, bioactive compounds are being investigated further (Dhama et al., 2020; Mani et al., 2020). There is a growing body of literature on the antiviral and immunomodulating properties of plant-based compounds, and their potential use as therapeutic agents against SARS-CoV-2 (Tiwari et al., 2018; Panyod et al., 2020; Tahir Ul Qamar et al., 2020). This includes traditional Chinese and traditional Indian medicinal compounds, vitamins, curcumin, glycyrrhizic acid, tea polyphenols and compounds derived from *Allium sativum* to name a few (Chen et al., 2020; Divya et al., 2020; Donma and Donma, 2020; Tripathi et al., 2020). Enhancing the bioavailability of natural compounds continues to be a challenge however, their structures can be used as scaffolds for the development of novel drugs (Ngwa et al., 2020).

In silico methods were used to compare the binding mode of naphthalene-based inhibitors (GRL-0617 and 3k) to dietary compounds including hypericin, rutin, cyanidin-3-O-glucoside and (-)-epigallocatechin gallate. The antimicrobial, anti-inflammatory and antioxidant activities of these phytochemicals have been reported and their structures may even be used as scaffolds in the drug development process (Mohammadi Pour et al., 2019). The aim was to determine whether the dietary compounds were able to bind in a similar manner as the positive control GRL-0617, and potentially interfere with the binding of ubiquitin. The results were validated further using *in vitro* assays.

MATERIALS AND METHODS

Protein Structures and Ligands

Several crystal structures of the SARS-CoV-2 PL^{pro} were obtained from the RCSB Protein Data Bank (PDB ID: 6xaa, 6w9c, 6wuu, 6wx4, and 7jrn) (Berman et al., 2000; Klemm et al., 2020; Osipiuk et al., 2020; Rut et al., 2020; Sacco et al., 2020). The SARS-CoV PL^{pro} (PDB ID: 4mm3) and MERS-CoV PL^{pro} (PDB ID: 4rf0) were also used for comparison in this study (Bailey-Elkin et al., 2014; Ratia et al., 2014). Crystallographic waters were removed and the native zinc ions were retained. A ubiquitin

chain was present in the structures of 6xaa, 4mm3, and 4rf0, which was used to generate two sets of docking data for each protein: PL^{pro} in complex with ubiquitin and, and apo PL^{pro} in the absence of ubiquitin. The ubiquitin in each complex was also isolated for protein-protein docking. The ligands that were used in this *in silico* study were the naphthalene inhibitors GRL-0617 and 3k, and the dietary compounds (-)-epigallocatechin gallate, cyanidin-3-O-glucoside, rutin and hypericin. The structures of the dietary compounds were obtained from the National Center for Biotechnology Information PubChem (Kim et al., 2019). GRL-0617 and 3k were drawn using Chem3D 19.0 (Perkin Elmer, Massachusetts, USA).

Molecular Docking Using the Schrödinger Suite

Molecular docking was performed using the Schrödinger Suite (Schrödinger, 2020a). The protein structures were prepared using the Protein Preparation Wizard, while the compounds were prepared using the LigPrep tool (Madhavi Sastry et al., 2013; Schrödinger, 2020b). The default settings were used for both of these steps and the optimized potentials for liquid simulations 3e (OPLS3e) force field was selected (Jorgensen and Tirado-Rives, 1988; Jorgensen et al., 1996; Shivakumar et al., 2010; Harder et al., 2016). The top ranking ligand conformation was selected for the subsequent molecular docking stage.

The residues that were within 5Å of the co-crystallized ligand GRL-0617 in the 7jrn structure were used to generate the receptor grid for each SARS-CoV-2 PL^{pro} (Friesner et al., 2004, 2006; Halgren et al., 2004; Schrödinger, 2020c). These residues were E167, K157, Y273, D164, G163, L162, C270, Q269, Y268, N267, G266, Y264, P248, P247, M208, and T301. To determine the corresponding residues in the SARS-CoV and MERS-CoV crystal structures, pairwise alignment was performed in the Multiple Sequence Viewer tool (Schrödinger, 2020a). The residues used to form the grid for SARS-CoV PL^{pro} were E168, K158, Y274, D165, G164, L163, C271, Q270, Y269, N268, G267, Y265, P249, P248, and M209. For MERS-CoV PL^{pro}, the receptor grid was generated based on the residues R1649, C1639, Y1760, D1646, D1645, P1644, V1757, A1756, T1755, E1754, G1752, F1750, P1731, T1730, V1691, and T1789.

The receptor grids were 20 × 20 × 20 Å in size and the OPLS3e force field was utilized. The compounds were then docked to each protein structure using the quantum-polarized ligand docking (QPLD) protocol, as previously described (Liang et al., 2020).

Blind Docking and the Prediction of Ligand-Binding Sites

The PL^{pro} crystal structures and the compounds were prepared as macromolecules and ligands in PyRx, respectively (Dallakyan and Olson, 2015). The corresponding.pdbqt files were obtained and the receptor grid was generated around the entire surface of the protein. The exhaustiveness was set to 2048. AutoDock Vina was used for molecular docking and the jobs were run on the cloud-computing server Galileo (Hypernet Labs) (Trott and Olson, 2010; Hypernet Labs Galileo, 2020). In addition to blind docking, the PrankWeb server was used to identify potential

binding pockets that were conserved in the 6xaa, 4mm3, and 4rf0 crystal structures (Jendele et al., 2019).

Protein-Protein Docking

The HDOCK server was used for ab initio template free protein-protein docking in this study (Yan et al., 2017, 2020). For the SARS-CoV-2, SARS-CoV, and MERS-CoV complexes, the main chain of PL^{pro} was defined as the receptor molecule, whereas the ubiquitin chain was the ligand. Protein-protein docking was also performed with PL^{pro} in the presence of compounds that were docked to the naphthalene-inhibitor site in the Schrödinger Suite. This was done for the 6xaa, 4mm3, and 4rf0 crystal structures in order to determine whether the presence of these ligands in the naphthalene-inhibitor region would affect the ability of ubiquitin to bind to PL^{pro}.
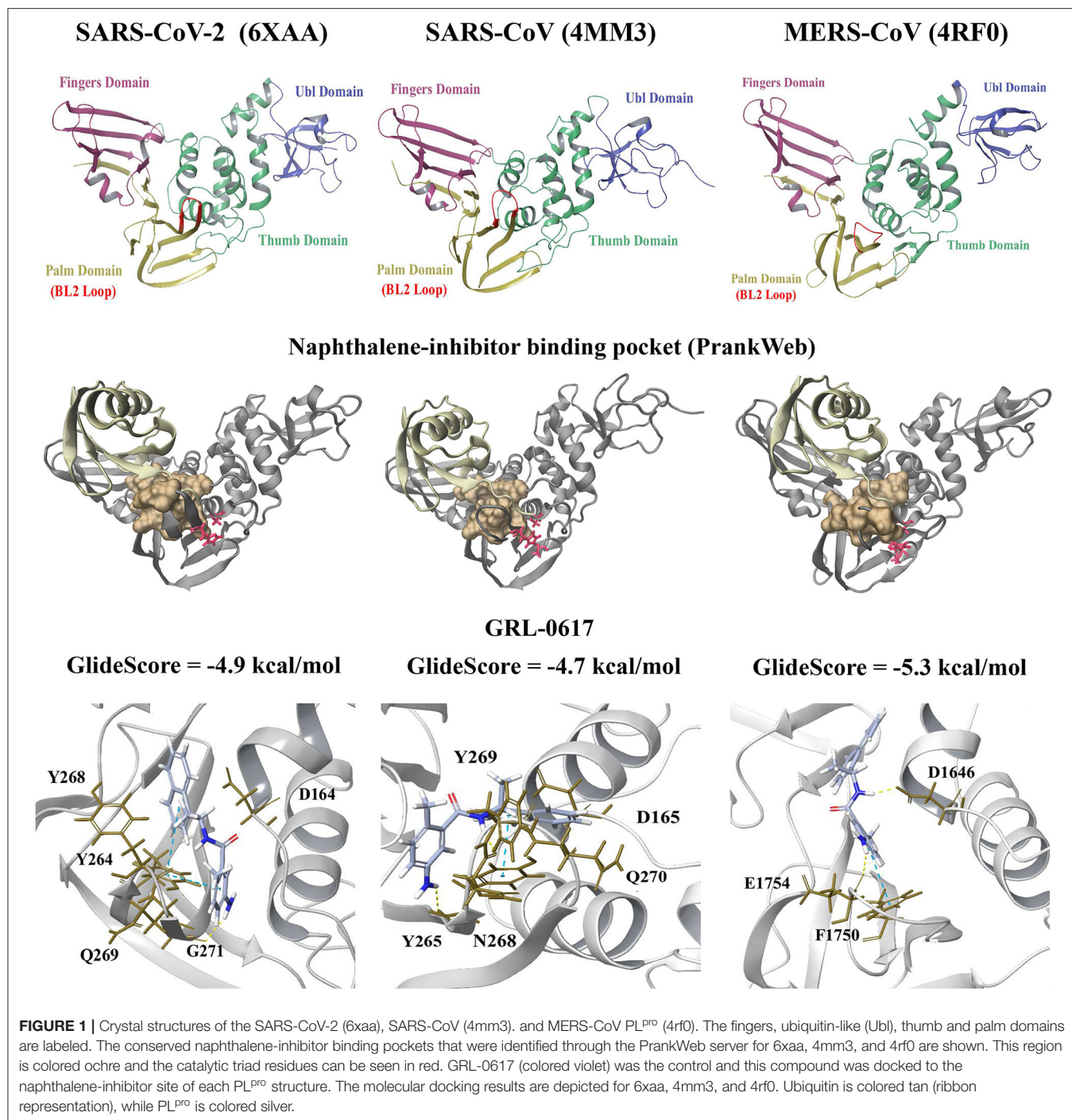
Enzymatic Activity Assay

In vitro inhibition of the PL^{pro} deubiquitinase activity was measured using a commercially available enzymatic activity assay (BP Bioscience, San Diego, CA, USA). The experiment was performed according to the manufacturer's instructions and all samples were assayed in triplicate. An excitation wavelength of 360 nm was used, and fluorescence was measured at an emission wavelength of 460 nm on the basis of the presence of a ubiquitinated fluoregenic substrate. The non-convalent inhibitor GRL-0617 was provided as an internal positive control and was used at concentration of 100 μM in the assay. We tested the following compounds for potential inhibition of PL^{pro} deubiquitinase activity: hypericin (89%, HWI pharma services GmbH, Germany), cyanidin-3-O-glucoside (reference standard, PhytoLab, Germany), and rutin (>94%), (-)-epicatechin gallate (>98%), (-)-epigallocatechin gallate (>95%), and cefotaxime (European pharmacopeia reference standard) from Sigma-Aldrich (St Luis, MO, USA); 20 mM stock solutions of each compound were stored at −80°C until use. Serial doubling dilutions were performed to yield a final concentration of 3.1 to 200 μM for assaying each compound. Readings (absolute fluorescence values at 1,200 gain), were made using a CLARIOstar® Plus fluorescence microplate reader (BMG Biotech, Oternberg, Germany). Where appropriate the % PL^{pro} deubiquitinase activity was calculated as the ratio of activity in the presence of inhibitor and total activity, and taking into account background readings.

RESULTS

Molecular docking was performed to examine the potential inhibitor behavior of dietary compounds and naphthalene inhibitors GRL-0617 and 3k on the SARS-CoV-2 PL^{pro}. Like SARS-CoV-2, SARS-CoV, and MERS-CoV are classified as betacoronaviruses and they predominantly affect the respiratory tract (Abdelrahman et al., 2020; Petersen et al., 2020). The PL^{pro} from the novel SARS-CoV-2 was consequently compared to the SARS-CoV and MERS-CoV PL^{pro} structures (**Figure 1**). In terms of the SARS-CoV and MERS-CoV PL^{pro}, the pairwise alignment revealed they had a sequence similarity of 89 and 50% with the SARS-CoV-2 PL^{pro},

FIGURE 1 | Crystal structures of the SARS-CoV-2 (6xaa), SARS-CoV (4mm3). and MERS-CoV PL^pro (4rf0). The fingers, ubiquitin-like (Ubl), thumb and palm domains are labeled. The conserved naphthalene-inhibitor binding pockets that were identified through the PrankWeb server for 6xaa, 4mm3, and 4rf0 are shown. This region is colored ochre and the catalytic triad residues can be seen in red. GRL-0617 (colored violet) was the control and this compound was docked to the naphthalene-inhibitor site of each PL^pro structure. The molecular docking results are depicted for 6xaa, 4mm3, and 4rf0. Ubiquitin is colored tan (ribbon representation), while PL^pro is colored silver.

respectively. The pairwise alignment was used to identify the corresponding residues of the naphthalene-inhibitor binding site for the SARS-CoV and MERS-CoV crystal structures. The three crystal structures (6xaa, 4mm3, and 4rf0) were analyzed using PrankWeb, a binding site prediction tool, which identified the naphthalene-inhibitor binding site as a conserved ligand binding pocket. This region was ranked as pocket 2, pocket 3 and pocket 2 in the SARS-CoV-2, SARS-CoV and MERS-CoV PL^pro structures, respectively (**Figure 1** and **Supplementary Table 1**).

GRL-0617 and 3k, as well as the dietary compounds were docked to the naphthalene-inhibitor binding site of the SARS-CoV-2 and SARS-CoV PL^pro structures. In the apo 6xaa crystal structure of SARS-CoV-2, the control compound

GRL-0617 docked to the naphthalene-inhibitor binding site with a GlideScore of −4.9 kcal/mol (**Figure 1**). It was predicted to form inter-atomic contacts with G271 (H-bond) and Y264 (π-π interactions). The GlideScore for the naphthalene-based inhibitor 3k was −2.4 kcal/mol and it also formed a π-π interaction with the PL^{pro} residue Y264 (**Figure 2**). In addition to Y264, a hydrogen bond with L162 was present in the ligand-interaction diagram. The molecular docking results demonstrated that the dietary compounds (-)-epigallocatechin gallate, cyanidin-3-O-glucoside, rutin and hypericin had strong binding affinities (**Figure 2**). These ligands formed a bond with Y268 (cyanidin-3-O-glucoside: H-bond, (-)-epigallocatechin gallate: H-bond, hypericin: π-π interaction, and rutin: H-bond). The protein residues Y264, T301, D164, R166, E167, K157, L162, G163, and Y273 were also involved in interactions with the ligands (**Figure 2**).

The GlideScores of the naphthalene-based inhibitors and the dietary compounds for the SARS-CoV and MERS-CoV PL^{pro} structures can be seen in **Figures 1**, **2**. Similar to docking to the same site in the SARS-CoV-2 PL^{pro}, the dietary ligands also had stronger binding affinities and formed a greater number of inter-atomic contacts with surrounding residues compared to GRL-0617 and 3k. GRL-0617 formed bonds with Y265 (H-bond and π-π interaction) and N268 (H-bond) in the SARS-CoV PL^{pro}, whereas these interactions were absent in docking with 3k (**Figures 1**, **2**). The residues Y265, Y269, Q270, Y274, D165, G164, and N268 were the most prominent amino acids involved in binding with (-)-epigallocatechin gallate, cyanidin-3-O-glucoside, hypericin and rutin (**Figure 2**). In regards to MERS-CoV, both GRL-0617 and 3k formed inter-atomic contacts with E1754 (GRL-0617: H-bond, 3k: H-bond), F1750 (GRL-0617: π-π interaction, 3k: π-π cation) and D1646 (GRL-0617: H-bond, 3k: salt bridge) (**Figures 1**, **2**). The dietary compounds also interacted with these residues, as well as D1645, G1758, A1756, G1729, and Y1760 (**Figure 2**).

Furthermore, blind docking was conducted on the 6xaa (SARS-CoV-2), 4mm3 (SARS-CoV), and 4rf0 (MERS-CoV) crystal structures in the absence of ubiquitin (**Figure 3** and **Supplementary Figures 1**, **2**). The blind docking results for the SARS-CoV-2 PL^{pro} can be seen in **Figure 3**. All six compounds had poses within the naphthalene-inhibitor binding site. For the SARS-CoV-2 and MERS-CoV PL^{pro}, all poses generated for (-)-epigallocatechin gallate were predicted to bind to this region (**Figure 3** and **Supplementary Figure 2**). The highest ranking pose that was positioned in the naphthalene-inhibitor binding pocket of the SARS-CoV-2 PL^{pro} was pose 1 for GRL-0617 (−8.0 kcal/mol), pose 4 for 3k (−7.5 kcal/mol), pose 1 for cyanidin-3-O-glucoside (−7.4 kcal/mol), pose 1 for (-)-epigallocatechin gallate (−8.1 kcal/mol), pose 1 for hypericin (−8.5 kcal/mol), and pose 1 for rutin (−7.6 kcal/mol). The binding affinities of the poses that were present in the naphthalene-inhibitor binding region for the 6xaa, 4mm3, and 4rf0 crystal structures can be found in **Supplementary Table 2**.

Moreover, the six compounds were docked to the 6wuu, 6w9c, 6wx4, and 7jrn crystal structures of the SARS-CoV-2 PL^{pro} (**Supplementary Figures 3–6**). With the exception of the 7jrn PL^{pro} structure, all of the dietary compounds had stronger
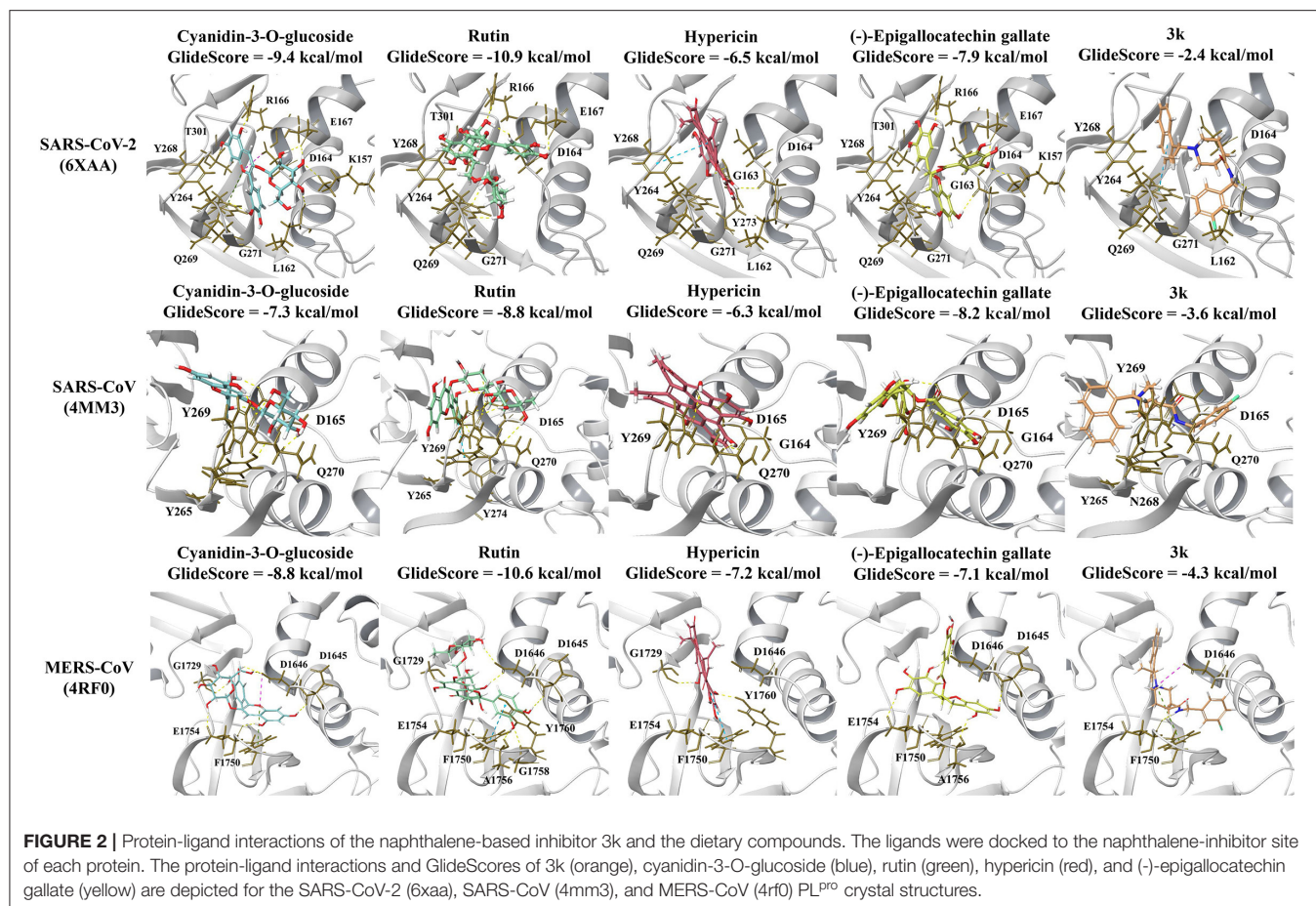
GlideScores than the naphthalene-based inhibitors. Hypericin, rutin and (-)-epigallocatechin gallate were predicted to bind more strongly than GRL-0617 to the 7jrn PL^{pro} structure, while cyanidin-3-O-glucoside had a similar GlideScore to the control compound. In the 6w9c, 6wuu, and 7jrn SARS-CoV-2 PLpro structures, 3k formed bonds with Y264 (6wuu: H-bond, 6w9c: H-bond, and salt bridge, 7jrn: salt bridge). In 7jrn, 3k formed a hydrogen bond with Y268. The intermolecular bonds that GRL-0617 formed with the protein residues varied amongst the crystal structures. GRL-0617 formed two hydrogen bonds with G266 and N267 in 6w9c, whereas a hydrogen bond was present with D164 in 6wuu. In 6wx4, there were two π-π interactions with Y264 and hydrogen bonds with G271 and Y268. There were π-π interactions with Y268 in 7jrn and a hydrogen bond with Q269.

Compared to GRL-0617 and 3k, the ligands rutin, cyanidin-3-O-glucoside and (-)-epigallocatechin gallate formed a greater number of inter-atomic contacts with the protein residues (**Supplementary Figures 3–6**). In 6w9c, the dietary compounds formed hydrogen bonds with D164. Hydrogen bonds were also present with D164 for (-)-epigallocatechin gallate and rutin in the 6wuu and 7jrn structures. The amino acid Y268 was also frequently involved in intermolecular bonds with the dietary compounds. This included (-)-epigallocatechin gallate (6w9c: H-bond), cyanidin-3-O-glucoside (6wuu: H-bond, 7jrn: π-π interaction), rutin (6wuu: H-bond and 6wx4: H-bond), and hypericin (6wx4: π-π interaction and 7jrn: π-π interactions). In the 7jrn PL^{pro}, hypericin also formed a hydrogen bond with Q269 and this was similar to the control compound. The blind docking results for the 6xaa, 6w9c, 6wx4, and 7jrn SARS-CoV-2 PL^{pro} crystal structures can be found in **Supplementary Table 3**.

Molecular docking was also performed on the SARS-CoV-2, SARS-CoV and MERS-CoV PL^{pro} structures with the ubiquitin chain present (**Figure 4**). When GRL-0617, 3k, (-)-epigallocatechin gallate, rutin, cyanidin-3-O-glucoside, and hypericin were docked to PL^{pro}, it was evident that they were binding distant from the naphthalene-inhibitor binding site. The position and orientation of these ligands, as well as their GlideScores, differed to when ubiquitin was absent (**Figure 4** and **Supplementary Table 4**). GRL-0617 in the SARS-CoV-2 PL^{pro}, for example, was found to form hydrogen bonds with P248 and G266. The control compound was no longer binding to the pocket that the C-terminal chain of ubiquitin extends into. Interestingly, hypericin was not able to bind in the presence of ubiquitin. Similarly, the blind docking results for PL^{pro} in complex with ubiquitin revealed that the compounds that originally had poses within the naphthalene-inhibitor binding site were displaced from this region.

The PL^{pro}-ubiquitin complexes were investigated further using the HDOCK server for protein-protein docking (**Figure 5**). The ubiquitin chain from each complex was isolated and was re-docked to the main PL^{pro} structure. There was a clear overlap in the position between the top ranked model of the docked ubiquitin and the crystallographic ubiquitin. The root-mean square deviation (RMSD) values that were generated from protein-protein docking were 0.4, 0.6, and 0.5 Å for the SARS-CoV-2, SARS-CoV, and MERS-CoV complexes, respectively, and importantly, the C-terminal tail of ubiquitin extended
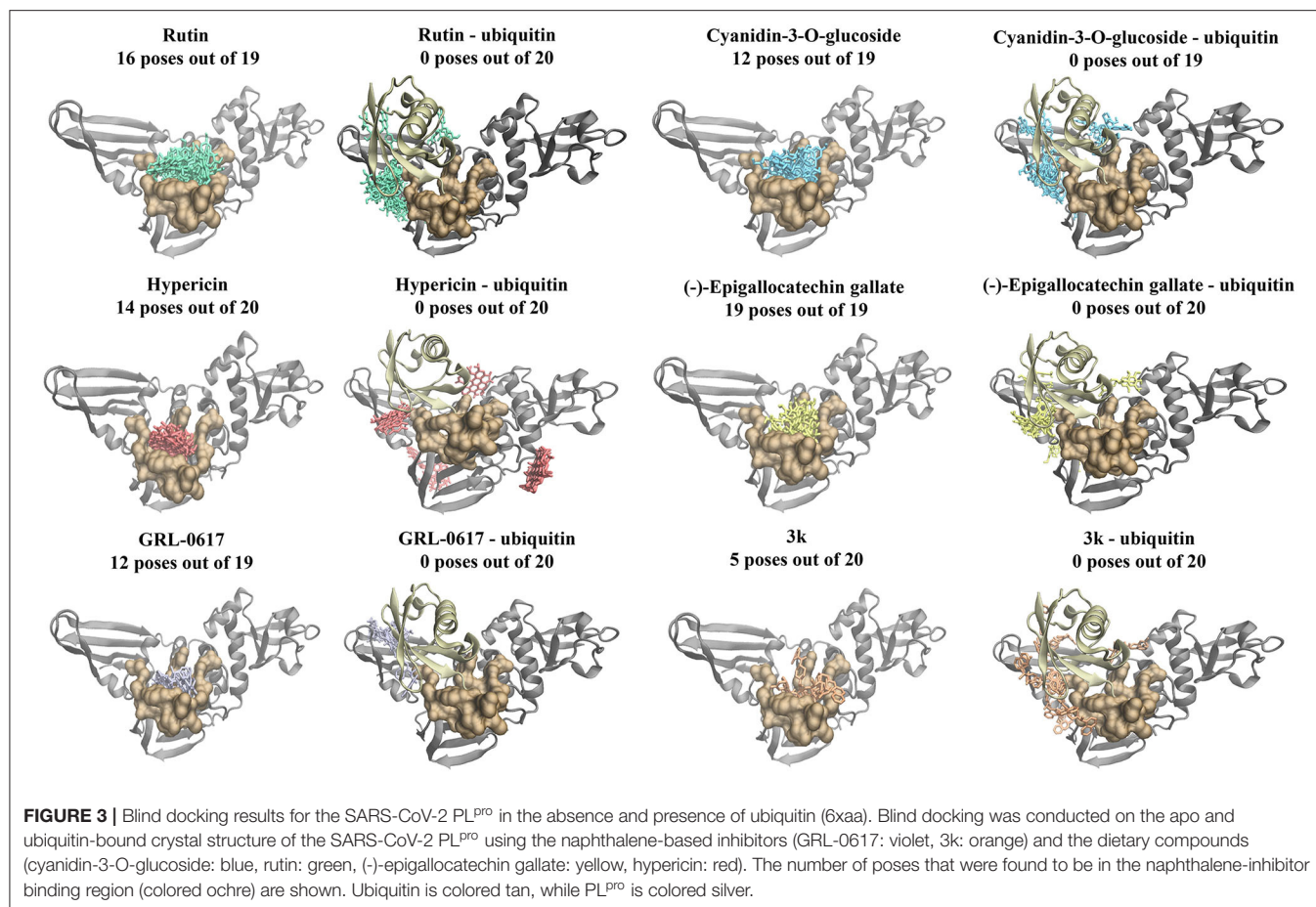
FIGURE 2 | Protein-ligand interactions of the naphthalene-based inhibitor 3k and the dietary compounds. The ligands were docked to the naphthalene-inhibitor site of each protein. The protein-ligand interactions and GlideScores of 3k (orange), cyanidin-3-O-glucoside (blue), rutin (green), hypericin (red), and (-)-epigallocatechin gallate (yellow) are depicted for the SARS-CoV-2 (6xaa), SARS-CoV (4mm3), and MERS-CoV (4rf0) PL^{pro} crystal structures.

into the catalytic and naphthalene binding region of PL^{pro}. The C-terminus of ubiquitin in the SARS-CoV-2, SARS-CoV and MERS-CoV PL^{pro} consists of residues R72, L73, R74, and G75. The C-terminal residue of ubiquitin is AYE76, GLZ76, and 3CN101 in the SARS-CoV-2, SARS-CoV and MERS-CoV structures, respectively. These three residues form a covalent bond with the catalytic cysteine residues and this is critical for deubiquitinase activity (C111 in SARS-CoV-2: 1.67 Å, C112 in SARS-CoV: 1.72 Å and C1592 in MERS-CoV: 1.45 Å). The 1.67, 1.72, and 1.45 Å correspond to the distances between the sulfur atom of the catalytic cysteine residue and the C-terminal ubiquitin residue in the crystal structures. Although non-covalent protein-protein docking was performed in the present study, the distance between AYE76 and C111 in SARS-CoV-2 was 1.94 Å. The distance between GLZ76 and residue C112 in SARS-CoV was 2.05 Å. Likewise, the distance between 3CN101 and C1592 in MERS-CoV was 1.48 Å.

In order to examine the ability of ubiquitin to bind to PL^{pro} when compounds are present in the naphthalene-inhibitor binding site, the ligands that were docked using the Schrödinger Suite were retained in the protein structures (**Figure 5**). When GRL-0617, 3k, (-)-epigallocatechin gallate, rutin, cyanidin-3-O-glucoside, and hypericin were bound to this region, dramatic

differences were observed in the binding mode of ubiquitin. The C-terminal chain of ubiquitin was no longer extending into the pocket that is located just above the catalytic triad. There were consequently changes in the position and orientation of ubiquitin for each ligand. When comparing the docked ubiquitin chain to the ubiquitin present in the original crystal structure, the RMSD values and docking scores were different (**Supplementary Table 5**). This was apparent for the SARS-CoV-2, SARS-CoV and MERS-CoV complexes.

Hypericin, Rutin, and Cyanidin-3-O-Glucoside Inhibit PL^{pro} Deubiquitinase Activity in a Concentration-Dependent Manner

Inhibition of PL^{pro} deubiquitinase activity by small molecules *in vitro* was investigated using an enzymatic assay. Overall, the findings indicate that hypericin, rutin, and cyanidin-3-O-glucoside resulted in a concentration-dependent inhibition of PL^{pro} deubiquitinase activity, with hypericin clearly highlighting the most potent inhibition of the test ligands (**Figure 6A**). At the higher concentrations ($>50 \mu M$) hypericin inhibited PL^{pro} deubiquitinase activity to a level akin to the internal

FIGURE 3 | Blind docking results for the SARS-CoV-2 PL^pro in the absence and presence of ubiquitin (6xaa). Blind docking was conducted on the apo and ubiquitin-bound crystal structure of the SARS-CoV-2 PL^pro using the naphthalene-based inhibitors (GRL-0617: violet, 3k: orange) and the dietary compounds (cyanidin-3-O-glucoside: blue, rutin: green, (-)-epigallocatechin gallate: yellow, hypericin: red). The number of poses that were found to be in the naphthalene-inhibitor binding region (colored ochre) are shown. Ubiquitin is colored tan, while PL^pro is colored silver.

positive control (GRL-0617), which was used at $100\,\mu M$ in the assay. Indeed, calculation of the percentage inhibition of PL^pro deubiquitinase activity at $100\,\mu M$ for each ligand highlighted the equivalence of GRL-0617 and hypericin in the assay (inhibition of activity by ∼90% by both compounds, **Figure 6B**). The findings indicate that at $100\,\mu M$ both rutin (∼50% inhibition) and cyanidin-3-O-glucoside (∼42% inhibition), can also be considered as potentially useful inhibitors of PL^pro deubiquitinase activity. The epicatechins (epigallocatechin gallate, ∼14% and epicatechin gallate, ∼20%), and cefotaxime (∼2%), yielded more modest effects.
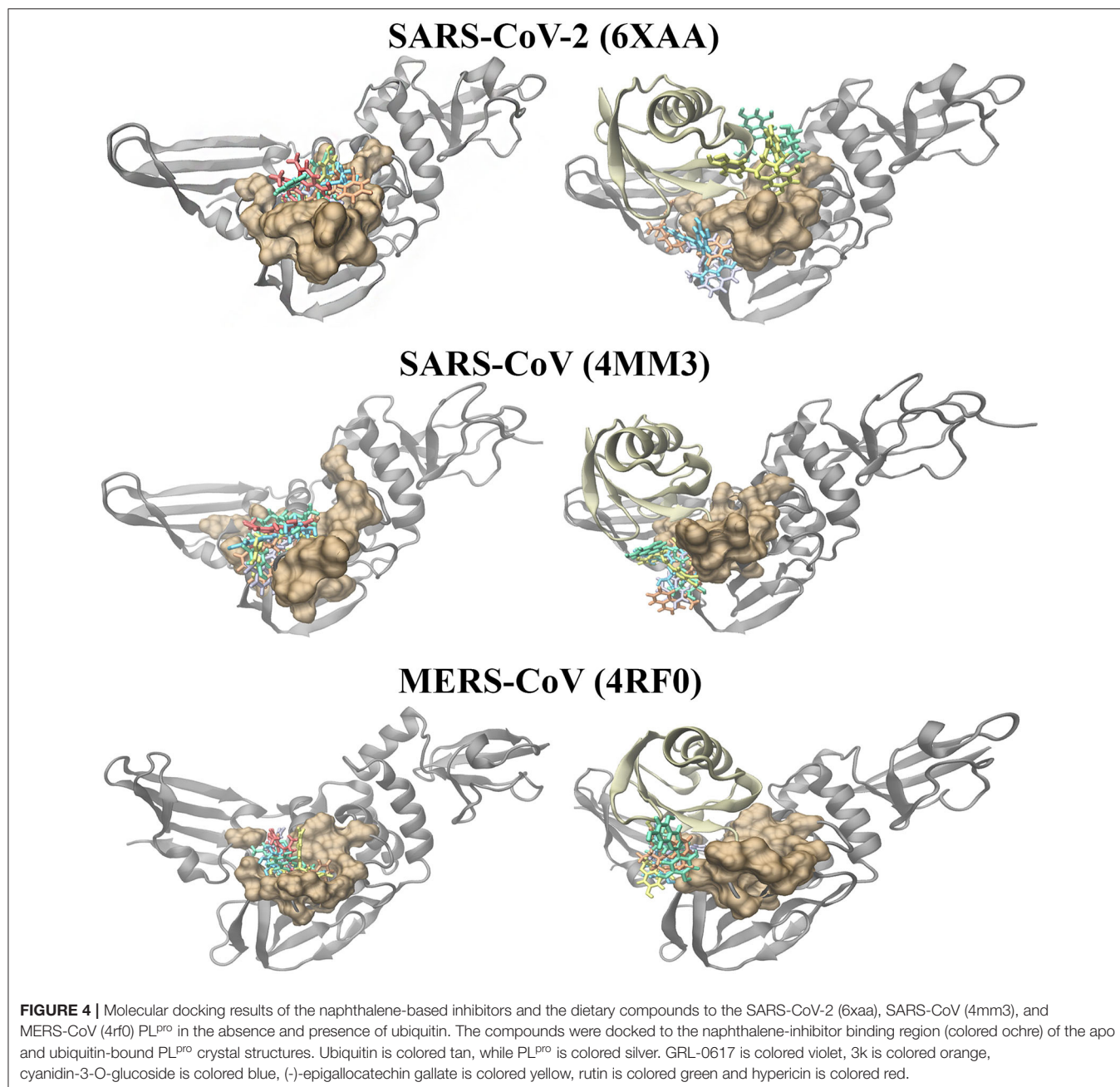
DISCUSSION

The innate immune system is the first line of defense against foreign pathogens and various cellular and molecular components are involved in this process (Liu et al., 2016; Huang et al., 2019). Post-translational modifications are also important regulators of immunity and this includes ubiquitination (Liu et al., 2016). Ubiquitin is a 76-amino acid polypeptide that can covalently interact with target proteins and ubiquitin itself can undergo ubiquitination at certain residues (Ciechanover et al., 2000; Pickart, 2001; Jiang and Chen, 2011). This results in

the formation of lysine-linked polyubiquitin chains or linear polyubiquitin chains (Heaton et al., 2015). It is well-known that lysine 48 (K48)-linked polyubiquitylation promotes the proteasomal degradation of target proteins (Ciechanover et al., 2000). Conversely, lysine 63 (K63)-linked polyubiquitylation has been implicated in cellular processes such as the DNA damage response, inflammation and endocytosis (Panier and Durocher, 2009; Erpapazoglou et al., 2014; Zhou Z. et al., 2020). It is also important to note that other types of polyubiquitin chain linkages are being explored and that ubiquitin modifications can lead to different cellular outcomes (Komander and Rape, 2012; Ohtake et al., 2018).

Moreover, human deubiquitinases (DUBs) are enzymes that remove ubiquitin modifications and they contribute to homeostasis (Li et al., 2016). Viruses are dependent on host cells for their survival and in order to complete their life cycle, they have developed strategies to evade the antiviral immune response (Nelemans and Kikkert, 2019). Interestingly, several viral proteins have been found to possess deubiquitinating activity and they can be used to antagonize or modulate the antiviral immune signaling pathway (Kumari and Kumar, 2018).

The deubiquitinating activity of the SARS-CoV-2 PL^pro was the main focus of this study and the crystal structure of
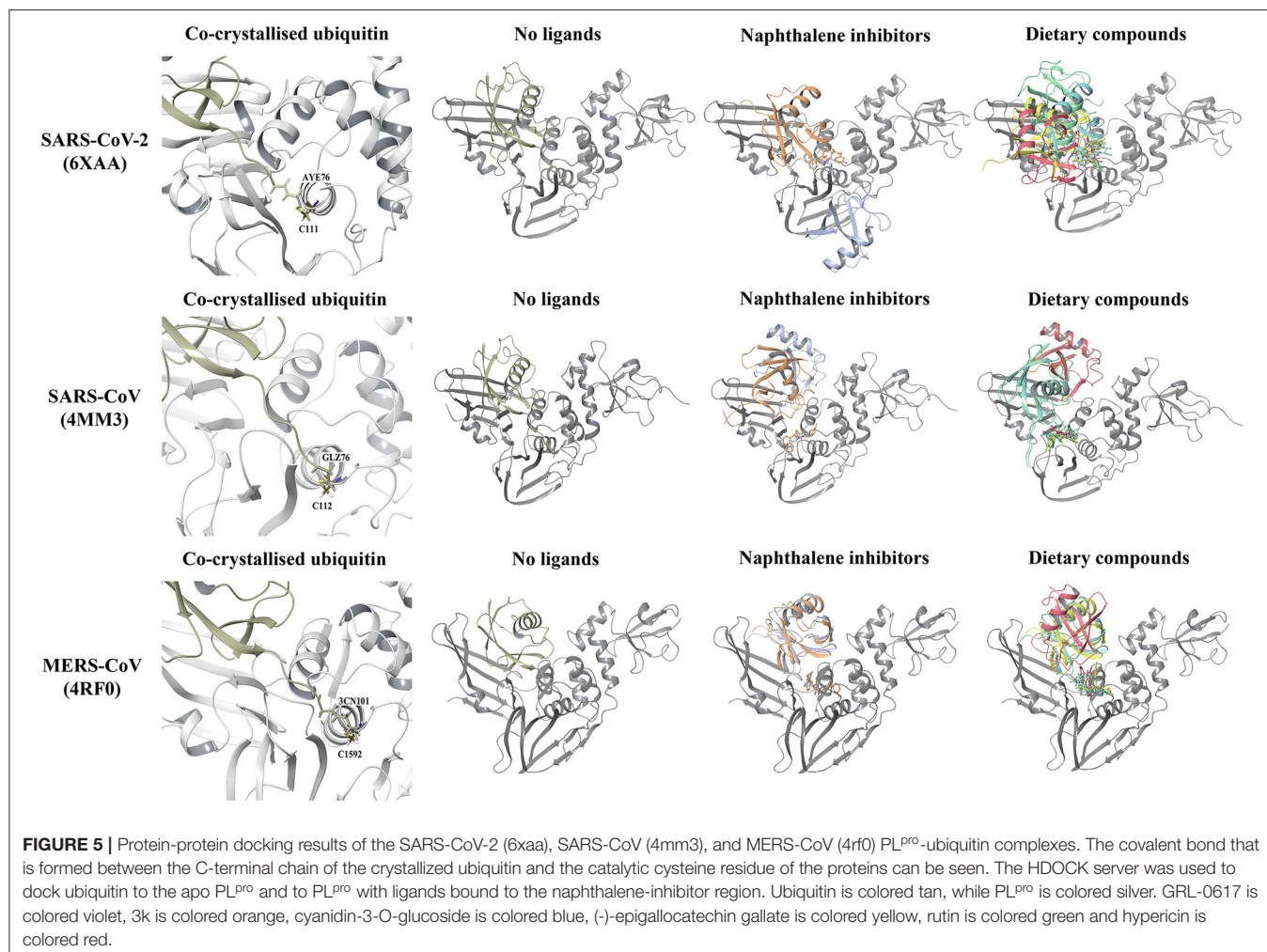
FIGURE 4 | Molecular docking results of the naphthalene-based inhibitors and the dietary compounds to the SARS-CoV-2 (6xaa), SARS-CoV (4mm3), and MERS-CoV (4rf0) PL^{pro} in the absence and presence of ubiquitin. The compounds were docked to the naphthalene-inhibitor binding region (colored ochre) of the apo and ubiquitin-bound PL^{pro} crystal structures. Ubiquitin is colored tan, while PL^{pro} is colored silver. GRL-0617 is colored violet, 3k is colored orange, cyanidin-3-O-glucoside is colored blue, (-)-epigallocatechin gallate is colored yellow, rutin is colored green and hypericin is colored red.

PL^{pro} in complex with ubiquitin propargylamide was utilized (Klemm et al., 2020). In addition to this, four other crystal structures of SARS-CoV-2 that were available on the RCSB PDB were evaluated. The crystal structures of the SARS-CoV PL^{pro}-ubiquitin aldehyde and MERS-CoV PL^{pro}-ubiquitin complexes were used for comparison (Bailey-Elkin et al., 2014; Ratia et al., 2014). Molecular docking allowed for the binding properties of compounds to the known target site of naphthalene-based inhibitors to be predicted and examined.

GRL-0617 was the control and this has previously been found to potently inhibit the SARS-CoV and SARS-CoV-2 PL^{pro} in a non-covalent manner (Ratia et al., 2008; Freitas

et al., 2020; Shin et al., 2020). The GRL-0617 inhibitor occupies the S3 and S4 pockets of the SARS-CoV and SARS-CoV-2 PL^{pro} (Ratia et al., 2008; Gao et al., in press). Based on the molecular docking results from the current study, GRL-0617 was predominantly surrounded by hydrophobic residues in the SARS-CoV and SARS-CoV-2 crystal structures (**Figure 1** and **Supplementary Figures 3–6**) (Ratia et al., 2008). This ligand was predicted to form inter-atomic contacts with the protein residues and this included D164 in the 6wuu SARS-CoV-2 structure, as well as Q269 in the 7jrn SARS-CoV-2 structure. In the crystal structure determined by Gao et al., GRL-0617, which was the co-crystallized ligand, was found to form hydrogen bonds with these

FIGURE 5 | Protein-protein docking results of the SARS-CoV-2 (6xaa), SARS-CoV (4mm3), and MERS-CoV (4rf0) PL^{pro}-ubiquitin complexes. The covalent bond that is formed between the C-terminal chain of the crystallized ubiquitin and the catalytic cysteine residue of the proteins can be seen. The HDOCK server was used to dock ubiquitin to the apo PL^{pro} and to PL^{pro} with ligands bound to the naphthalene-inhibitor region. Ubiquitin is colored tan, while PL^{pro} is colored silver. GRL-0617 is colored violet, 3k is colored orange, cyanidin-3-O-glucoside is colored blue, (-)-epigallocatechin gallate is colored yellow, rutin is colored green and hypericin is colored red.
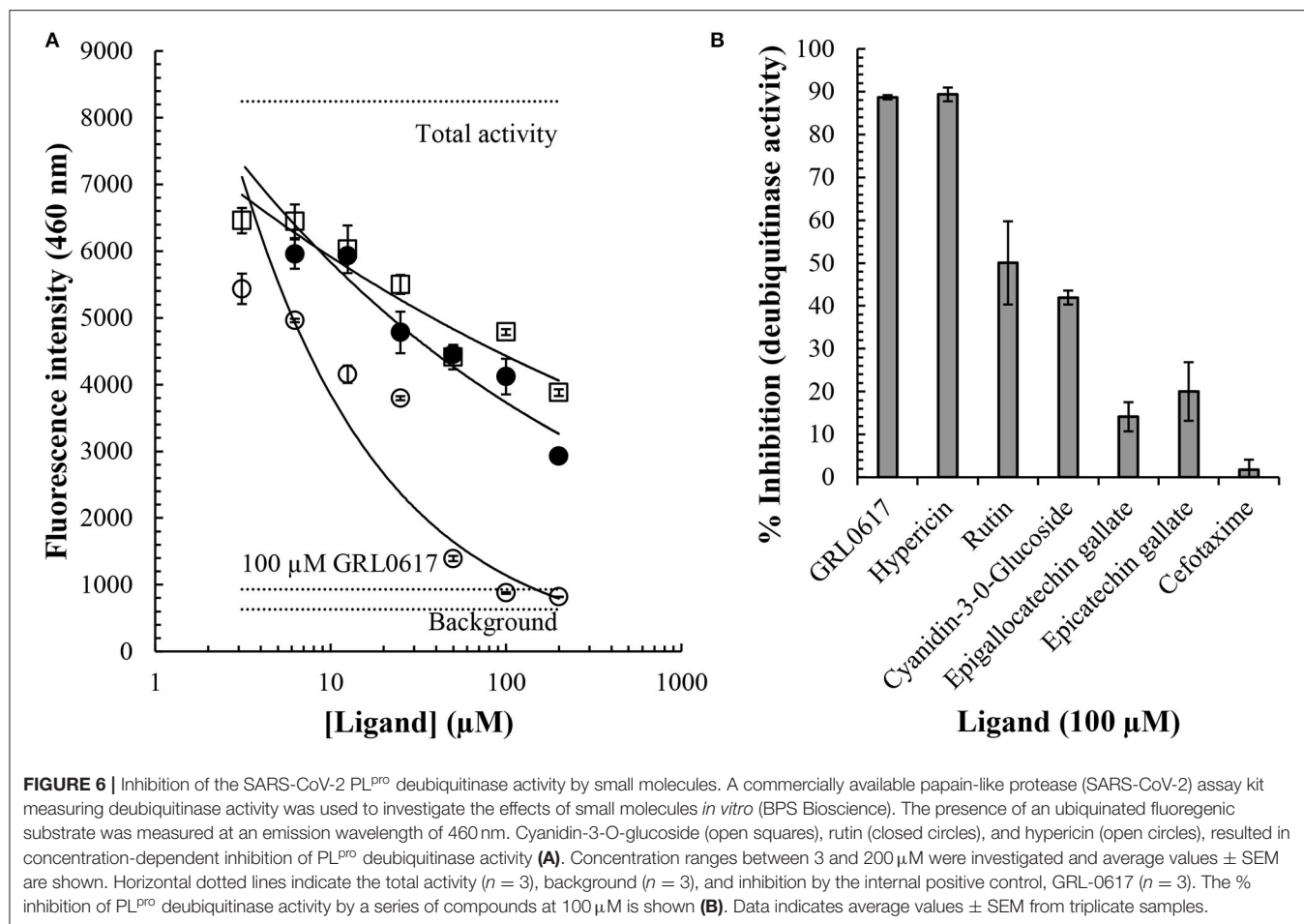
critical residues (Gao et al., in press). In saying this, D164 and Q269 were found to surround GRL-0617 in the 6xaa, 6w9c, and 6wx4 structures of the SARS-CoV-2 PL^{pro}.

GRL-0617 also interacted with Y268 in the SARS-CoV-2 PL^{pro} and inter-atomic contacts were present with this residue in some structures. Interestingly, the naphthalene-based inhibitor 3k was found to consistently form inter-atomic contacts with Y264 in all of the SARS-CoV-2 crystal structures (**Figure 2** and **Supplementary Figures 3–6**) (Bosken et al., 2020). Intermolecular bonds were also formed between 3k and D164 in three of the SARS-CoV-2 papain-like proteases, as well as Y268 in the 6wx4 structure (Bosken et al., 2020). Bosken et al. have identified these residues as playing an important role in the binding mode of 3k (Bosken et al., 2020).

The differences observed in the intermolecular bonds may be due to the conformations of the fingers domain and BL2 loop in the PL^{pro} crystal structures (**Figure 1**) (Báez-Santos et al., 2015). In the SARS-CoV-2 and SARS-CoV PL^{pro} structures, the BL2 loop corresponds to residues 267-272 (Lee et al., 2015; Gao et al., in press). In the MERS-CoV PL^{pro} structure used in this study, the BL2 loop is comprised of residues 1,752–1,758 (Bailey-Elkin

et al., 2014; Lee et al., 2015). The structural significance of the BL2 loop (blocking loop) has been discussed in a number of papers and its flexibility has been highlighted (Báez-Santos et al., 2015; Bosken et al., 2020; Klemm et al., 2020). Conformational changes have been observed in the BL2 loop and "open" or "closed" conformations have been reported in the literature (Báez-Santos et al., 2015). In regards to MERS-CoV, there are significant structural differences in the BL2 loop and it has been suggested that this affects inhibitor recognition specificity (Lee et al., 2015).

GRL-0617 is ineffective against MERS-CoV and in the study by Shin et al., it was discussed that this may be due to the presence of a threonine residue instead of tyrosine at a conserved position (Lee et al., 2015; Shin et al., 2020). In the SARS-CoV-2 and SARS-CoV PL^{pro} sequences, the corresponding residues are Y268 and Y269, respectively (Shin et al., 2020). Y268 is required for the inhibitory effect of GRL-0617 and Shin et al. demonstrated that mutating this residue strongly reduces its potency (Shin et al., 2020). While GRL-0617 and 3k were predicted to bind to the MERS-CoV PL^{pro} (4rf0) in this study, further docking to additional crystal structures may be required for comparison (**Figures 1**, **2**). The naphthalene-based inhibitors

FIGURE 6 | Inhibition of the SARS-CoV-2 PL^{pro} deubiquitinase activity by small molecules. A commercially available papain-like protease (SARS-CoV-2) assay kit measuring deubiquitinase activity was used to investigate the effects of small molecules *in vitro* (BPS Bioscience). The presence of an ubiquinated fluorogenic substrate was measured at an emission wavelength of 460 nm. Cyanidin-3-O-glucoside (open squares), rutin (closed circles), and hypericin (open circles), resulted in concentration-dependent inhibition of PL^{pro} deubiquitinase activity **(A)**. Concentration ranges between 3 and 200 μM were investigated and average values ± SEM are shown. Horizontal dotted lines indicate the total activity ($n = 3$), background ($n = 3$), and inhibition by the internal positive control, GRL-0617 ($n = 3$). The % inhibition of PL^{pro} deubiquitinase activity by a series of compounds at 100 μM is shown **(B)**. Data indicates average values ± SEM from triplicate samples.

were surrounded by the residues D165, Y269, and Q270 in the SARS-CoV PL^{pro}. Ratia et al. and Báez-Santos et al., have also described the importance of these residues in the mechanisms of action of these ligands (Ratia et al., 2008; Báez-Santos et al., 2014).

Most notably, the dietary compounds (-)-epigallocatechin gallate, hypericin, rutin and cyanidin-3-O-glucoside were predicted to bind more strongly to the naphthalene-inhibitor site of the SARS-CoV-2, SARS-CoV, and MERS-CoV papain-like proteases than the known inhibitors (**Figure 2** and **Supplementary Figures 3–6**). They also formed multiple interactions with the key protein residues compared to GRL-0617 and 3k. Similarly, the blind docking results on the main PL^{pro} chains showed that these natural ligands had multiple poses within this region (**Figure 3** and **Supplementary Figures 1, 2**). (-)-Epigallocatechin gallate, rutin and cyanidin-3-O-glucoside are flavonoids, a biologically active class of the phenolic compounds (Bonvino et al., 2018). In a recent literature review conducted by Verma et al., the flavonoids were found to be the largest class of compounds with potential activity against coronaviruses (Verma et al., 2020).

In 2005, Li et al. published a study about the antiviral activities of natural compounds against SARS-CoV (Li et al., 2005). Lycorine was identified as a potent antiviral compound and potentially a candidate for the development of new medicines (Li et al., 2005). Natural compounds have been screened for their ability to target SARS-CoV-2 proteins. This includes extracts of medicinal herbs and several studies have focused on their inhibitory effects on key proteins, such as the spike glycoprotein and the main protease (M^{pro}) (Mani et al., 2020; Pitsillou et al., 2020; Russo et al., 2020; Smith and Smith, 2020). In a recent paper by Alamri et al. a structured-based computational approach was utilized to identify compounds that may act as pan-PL^{pro} inhibitors and could be developed further as antiviral agents (Alamri et al., in press). Given the current situation, *in silico* methods have made it possible for large libraries of existing approved compounds to be screened in a relatively fast manner (Ojha et al., 2020). The structures of the hits identified from these computational studies could be optimized as part of the drug discovery process (Ojha et al., 2020). In addition to synthetic pharmacological compounds, herbal constituents can be screened in the same manner and this method has been described in many papers (Bhowmik et al., 2020; Chikhale et al., 2020; Ghosh et al., 2020; Gupta et al., 2020; Jena et al., 2020; Krupanidhi et al., 2020; Muhseen et al., 2020; Sinha et al.,

2020; Subbaiyan et al., 2020). A number of studies that can be found on the World Health Organization's International Clinical Trials Registry Platform also involve plant-based compounds, particularly flavonoids.

Ratia et al. determined the crystal structure of SARS-CoV in complex with ubiquitin aldehyde and they described how this polypeptide interacts with the palm and fingers regions of PL^{pro} (Ratia et al., 2014). They emphasized that a significant amount of the binding energy of ubiquitin can be attributed to its C-terminal residues (R72-G76) and that this portion of ubiquitin forms an extensive number of intermolecular hydrogen bonds with PL^{pro} (Ratia et al., 2014). The results from their study also indicated that the SARS-CoV PL^{pro} had a preference for K48-linked ubiquitin and ISG15, over K63-polyubiquitin chains and mono-ubiquitin (Ratia et al., 2014). Most notably, two recognition sites on the surface of PL^{pro} were characterized and were defined as either SUb1 or SUb2 (Ratia et al., 2014).

In the SARS-CoV-2 PL^{pro} complex, ubiquitin propargylamide sits on the same subdomains as the SARS-CoV structure (palm and fingers regions), and the C-terminus extends into the active site (Klemm et al., 2020). Like SARS-CoV, the SARS-CoV-2 PL^{pro} was also found to have a second ubiquitin binding site (SUb2) that is important for the binding of polyubiquitin (K48-diubiquitin) and ISG15 (Klemm et al., 2020). The MERS-CoV (space group P6$_5$22) PL^{pro}-ubiquitin complex was solved by Bailey-Elkin et al. and in their paper, they refer to this structure as the closed conformation since the fingers domain is shifted toward the ubiquitin (Bailey-Elkin et al., 2014).

When ubiquitin was present in the SARS-CoV-2, SARS-CoV and MERS-CoV PL^{pro} structures, the results from Schrödinger and blind docking showed that compounds were displaced from the naphthalene-inhibitor binding pocket (**Figures 3**, **4** and **Supplementary Figures 1, 2**). Compared to the apo PL^{pro}, hypericin was unable to produce molecular docking poses for the PL^{pro}-ubiquitin complexes. Likewise, the protein-protein docking results with the ligands already bound to this region in PL^{pro} revealed that ubiquitin was binding in different conformations and that the position of the C-terminus was altered (**Figure 5**). This suggests that the dietary compounds may be able to interfere with the deubiquitinase activity of PL^{pro} and in terms of *in silico* methods, this can be evaluated further using molecular dynamics (MD) simulations.

A commercially available PL^{pro} enzymatic assay was used to measure deubiquitinase activity using GRL-0617 as an internal positive control; in this specific assay GRL-0617 has been shown to have an IC$_{50}$ value of 1.7 μM for inhibition of PL^{pro} deubiquitinase activity (BP Bioscience). Overall, our findings indicated inhibition with an order of potency of GRL-0617 and hypericin > rutin and cyanidin-3-O-glucoside > epigallocatechin gallate and epicatechin gallate >> cefotaxime. GRL-0617 and hypericin > rutin > cyanidin-3-O-glucoside and epicatechin gallate > cefotaxime and epigallocatechin gallate (**Figure 6**). The potent inhibition of PL^{pro} deubiquitinase activity by hypericin which, at higher concentrations, was analogous to GRL-0617, is particularly encouraging. Hypericin is an anthraquinone derivative that

can be found in the flowering plant *Hypericum perforatum*, which is also commonly known as St. John's Wort (Napoli et al., 2018). It has been identified as a lead compound for the SARS-CoV-2 spike protein and its antiviral properties have been the subject of numerous papers in the past (Jacobson et al., 2001; Shih et al., 2018; Chen et al., 2019). In addition to its antiviral effects, St. John's Wort is also being investigated for its antidepressant properties and synthetic hypericin (SGX301) has gained attention for its use as a photodynamic agent in the treatment of cutaneous T-cell lymphoma (Rook et al., 2010; Montoya et al., 2015; Apaydin et al., 2016).

While specific compounds were selected for use in this study, it would be important to expand this in the future to incorporate a greater number of phytochemicals that are present in various plant extracts. Network pharmacology is also being increasingly used in drug discovery and this systematic approach can assist with identifying potential protein targets and lead compounds, as well as understanding their mechanisms of action (Zhang et al., 2019; Pan H. D. et al., 2020). Nonetheless, the antiviral, antioxidant and anti-inflammatory properties of the compounds used in this study had been previously reported in the literature and were consequently suitable candidates. Molecular docking was used for virtual screening and although the scoring functions produced from docking aren't absolute binding energies, it allowed for predictions to be made about the protein-ligand interactions. Docking was performed using the Glide (XP) protocol of the Schrödinger Suite and in a study conducted by Wang et al., this was found to have a 90% success rate in identifying the correct binding poses of ligands (Wang et al., 2016). In this study, the inhibitory activities of the compounds were subsequently measured using an enzymatic activity assay. *In silico* tools are currently being utilized for the early stages of the drug discovery pipeline however, it is important to note that the pipeline involves multiple steps and is a time consuming process (Agostino et al., 2019). Potential drugs must be explored further in pre-clinical trials using a combination of techniques and clinical trials (Agostino et al., 2019).

CONCLUSION

Overall, on the basis of our *in silico* and *in vitro* evaluations, hypericin, rutin, and cyanidin-3-O-glucoside can be considered potential lead compounds. In particular, further clarification of the molecular mechanisms and antiviral properties of hypericin, which displayed high potency in the *in vitro* assay and favorable binding properties in the *in silico* studies, is warranted.

DATA AVAILABILITY STATEMENT

The original contributions presented in the study are included in the article/**Supplementary Material**, further inquiries can be directed to the corresponding author/s.

AUTHOR CONTRIBUTIONS

TK and AH conceptualized the aims and methodology and were involved in supervision. TK was involved in the production of the first draft of the manuscript. EP performed data analysis, data curation, and was involved in production of the first draft of the manuscript. JL was involved in data analysis and curation and was involved in production of the first draft of the manuscript. KV performed formal data analysis and was involved in data curation. KL performed formal data analysis and validation. All authors contributed to editing and reviewing the manuscript.

ACKNOWLEDGMENTS

SUPPLEMENTARY MATERIAL

The Supplementary Material for this article can be found online at: https://www.frontiersin.org/articles/10.3389/fchem.2020.623971/full#supplementary-material

Supplementary Figure 1 | Blind docking of the naphthalene-based inhibitors and dietary compounds to the SARS-CoV PL^{pro}.

Supplementary Figure 2 | Blind docking of the naphthalene-based inhibitors and dietary compounds to the MERS-CoV PL^{pro}.

Supplementary Figure 3 | Molecular docking results of the naphthalene-based inhibitors and dietary compounds for the SARS-CoV-2 PL^{pro} structure 6w9c.

Supplementary Figure 4 | Molecular docking results of the naphthalene-based inhibitors and dietary compounds for the SARS-CoV-2 PL^{pro} structure 6wuu.

Supplementary Figure 5 | Molecular docking results of the naphthalene-based inhibitors and dietary compounds for the SARS-CoV-2 PL^{pro} structure 6wx4.

Supplementary Figure 6 | Molecular docking results of the naphthalene-based inhibitors and dietary compounds for the SARS-CoV-2 PL^{pro} structure 7jrn.

Supplementary Table 1 | PrankWeb conservation analysis results for the SARS-CoV-2 (6xaa), SARS-CoV (4mm3), and MERS-CoV PL^{pro} (4rf0).

Supplementary Table 2 | Blind docking of the naphthalene-based inhibitors and dietary compounds to the SARS-CoV-2 (6xaa), SARS-CoV (4mm3), and MERS-CoV (4rf0) PL^{pro} structures.

Supplementary Table 3 | Blind docking of the naphthalene-based inhibitors and dietary compounds to the SARS-CoV-2 6w9c, 6wuu, 6wx4, and 7jrn PL^{pro} crystal structures. No poses were found in the naphthalene inhibitor site for GRL-0617 and hypericin in the 6wuu structure.

Supplementary Table 4 | The GlideScores (kcal/mol) of the naphthalene-based inhibitors and dietary compounds for the SARS-CoV-2, SARS-CoV, and MERS-CoV crystal structures with ubiquitin are listed.

Supplementary Table 5 | The docking scores and RMSD values for the top-ranked PL^{pro}-ubiquitin complexes from the HDOCK server are provided.

REFERENCES

Abdelrahman, Z., Li, M., and Wang, X. (2020). Comparative review of SARS-CoV-2, SARS-CoV, MERS-CoV, and influenza a respiratory viruses. *Front. Immunol.* 11:2309. doi: 10.3389/fimmu.2020.552909

Agostino, B., Gabriele, C., Luca, S., and Marco, R. (2019). The *in silico* drug discovery toolbox: applications in lead discovery and optimization. *Curr. Med. Chem.* 26, 3838–3873. doi: 10.2174/0929867324666171107101035

Alamri, M. A., Tahir ul Qamar, M., Mirza, M. U., Alqahtani, S. M., Froeyen, M., and Chen, L. L. (in press). Discovery of human coronaviruses pan-papain-like protease inhibitors using computational approaches. *J. Pharm. Anal.* doi: 10.1016/j.jpha.2020.08.012

Apaydin, E. A., Maher, A. R., Shanman, R., Booth, M. S., Miles, J. N. V., Sorbero, M. E., et al. (2016). A systematic review of St. John's wort for major depressive disorder. *Syst. Rev* 5:12. doi: 10.1186/s13643-016-0325-2

Báez-Santos, Y. M., Barraza, S. J., Wilson, M. W., Agius, M. P., Mielech, A. M., Davis, N. M., et al. (2014). X-ray structural and biological evaluation of a series of potent and highly selective inhibitors of human coronavirus papain-like proteases. *J. Med. Chem.* 57, 2393–2412. doi: 10.1021/jm401712t

Báez-Santos, Y. M., St John, S. E., and Mesecar, A. D. (2015). The SARS-coronavirus papain-like protease: structure, function and inhibition by designed antiviral compounds. *Antiviral Res.* 115, 21–38. doi: 10.1016/j.antiviral.2014.12.015

Bailey-Elkin, B. A., Knaap, R. C. M., Johnson, G. G., Dalebout, T. J., Ninaber, D. K., van Kasteren, P. B., et al. (2014). Crystal structure of the Middle East respiratory syndrome coronavirus (MERS-CoV) papain-like protease bound to ubiquitin facilitates targeted disruption of deubiquitinating activity to demonstrate its role in innate immune suppression. *J. Biol. Chem* 289, 34667–34682. doi: 10.1074/jbc.M114.609644

Bar-Zeev, N., and Moss, W. J. (2020). Encouraging results from phase 1/2 COVID-19 vaccine trials. *Lancet* 396, 448–449. doi: 10.1016/S0140-6736(20)31611-1

Berman, H. M., Westbrook, J., Feng, Z., Gilliland, G., Bhat, T. N., Weissig, H., et al. (2000). The protein data bank. *Nucleic Acids Res.* 28, 235–242. doi: 10.1093/nar/28.1.235

Bhowmik, D., Nandi, R., and Kumar, D. (2020). Evaluation of flavonoids as 2019-nCoV cell entry inhibitor through molecular docking and pharmacological analysis. *ChemRxiv [Preprint].* doi: 10.26434/chemrxiv.12071508

Bonvino, N. P., Liang, J., McCord, E. D., Zafiris, E., Benetti, N., Ray, N. B., et al. (2018). OliveNet^{TM}: a comprehensive library of compounds from *Olea europaea. Database* 2018:bay016. doi: 10.1093/database/bay016

Bosken, Y. K., Cholko, T., Lou, Y. C., Wu, K. P., and Chang C. E. A. (2020). Insights into dynamics of inhibitor and ubiquitin-like protein binding in SARS-CoV-2 papain-like *protease. Front. Mol. Biosci.* 7:174. doi: 10.3389/fmolb.2020.00174

Chen, H., Muhammad, I., Zhang, Y., Ren, Y., Zhang, R., Huang, X., et al. (2019). Antiviral activity against infectious bronchitis virus and bioactive components of *Hypericum Perforatum L. Front. Pharmol.* 10:1272. doi: 10.3389/fphar.2019.01272

Chen, L., Hu, C., Hood, M., Zhang, X., Zhang, L., Kan, J., et al. (2020). A novel combination of vitamin C, curcumin and glycyrrhizic acid potentially regulates immune and inflammatory response associated with coronavirus infections: a perspective from system biology analysis. *Nutrients* 12:1193. doi: 10.3390/nu12041193

Chikhale, R. V., Gurav, S. S., Patil, R. B., Sinha, S. K., Prasad, S. K., Shakya, A., et al. (2020). Sars-cov-2 host entry and replication inhibitors from Indian ginseng: an *in-silico* approach.

J. Biomol. Struct. Dyn. 2020, 1–12. doi: 10.1080/07391102.2020.177
8539

Ciechanover, A., Orian, A., and Schwartz, A. L. (2000). Ubiquitin-mediated
proteolysis: biological regulation via destruction. Bioessays 22, 442–451. doi: 10.
1002/(SICI)1521-1878(200005)22:5<442::AID-BIES6>3.0.CO;2-Q

Coronaviridae Study Group of the International Committee on Taxonomy
of Viruses (2020). The species severe acute respiratory syndrome-related
coronavirus: classifying 2019-nCoV and naming it SARS-CoV-2. Nat.
Microbiol. 5, 536–544. doi: 10.1038/s41564-020-0695-z

Dallakyan, S., and Olson, A. J. (2015). "Small-molecule library screening by
docking with PyRx," in Chemical Biology: Methods and Protocols, eds J. E.
Hempel, C.H. Williams, and C. C. Hong (New York, NY: Springer New
York), 243–250.

de la Rica, R., Borges, M., and Gonzalez-Freire, M. (2020). COVID-19: in the eye of
the cytokine storm. Front. Immunol. 11:2313. doi: 10.3389/fimmu.2020.558898

Dhama, K., Khan, S., Tiwari, R., Sircar, S., Bhat, S., Malik, Y. S., et al. (2020).
Coronavirus disease 2019–COVID-19. Clin. Microbiol. Rev. 33:e00028-20.
doi: 10.1128/CMR.00028-20

Divya, M., Vijayakumar, S., Chen, J., Vaseeharan, B., and Durán-Lara, E.
F. (2020). South Indian medicinal plants can combat deadly viruses
along with COVID-19? - a review. Microb. Pathog. 2020:104277.
doi: 10.1016/j.micpath.2020.104277

Donma, M. M., and Donma, O. (2020). The effects of allium sativum on immunity
within the scope of COVID-19 infection. Med. Hypotheses 144:109934.
doi: 10.1016/j.mehy.2020.109934

Erpapazoglou, Z., Walker, O., and Haguenauer-Tsapis, R. (2014). Versatile
roles of k63-linked ubiquitin chains in trafficking. Cells 3, 1027–1088.
doi: 10.3390/cells3041027

FDA (2020). Approves First Treatment For Covid-19.

Folegatti, P. M., Ewer, K. J., Aley, P. K., Angus, B., Becker, S., Belij-
Rammerstorfer, S., et al. (2020). Safety and immunogenicity of the
ChAdOx1 nCoV-19 vaccine against SARS-CoV-2: a preliminary report
of a phase 1/2, single-blind, randomised controlled trial. Lancet 396, 467–478.
doi: 10.1016/S0140-6736(20)31604-4

Freitas, B. T., Durie, I. A., Murray, J., Longo, J. E., Miller, H. C., Crich, D., et al.
(2020). Characterization and noncovalent inhibition of the deubiquitinase and
deISGylase activity of SARS-CoV-2 papain-like protease. ACS Infect. Dis. 6,
2099–2109. doi: 10.1021/acsinfecdis.0c00168

Friesner, R. A., Banks, J. L., Murphy, R. B., Halgren, T. A., Klicic, J. J., Mainz, D.
T., et al. (2004). Glide: a new approach for rapid, accurate docking and scoring.
1. Method and assessment of docking accuracy. J. Med. Chem. 47, 1739–1749.
doi: 10.1021/jm0306430

Friesner, R. A., Murphy, R. B., Repasky, M. P., Frye, L. L., Greenwood, J. R.,
Halgren, T. A., et al. (2006). Extra precision glide: docking and scoring
incorporating a model of hydrophobic enclosure for protein–ligand complexes.
J. Med. Chem. 49, 6177–6196. doi: 10.1021/jm051256o

Gao, X., Qin, B., Chen, P., Zhu, K., Hou, P., Wojdyla, J. A., et al. (in press).
Crystal structure of SARS-CoV-2 papain-like protease. Acta Pharmaceut. Sin.
B. doi: 10.1016/j.apsb.2020.08.014

Ghosh, R., Chakraborty, A., Biswas, A., and Chowdhuri, S. (2020). Evaluation
of green tea polyphenols as novel corona virus (SARS CoV-2) main protease
(Mpro) inhibitors - an in silico docking and molecular dynamics simulation
study. J. Biomol. Struct. Dyn. 2020, 1–13. doi: 10.1080/07391102.2020.17
79818

Gupta, S., Singh, A. K., Kushwaha, P. P., Prajapati, K. S., Shuaib, M., Senapati, S.,
et al. (2020). Identification of potential natural inhibitors of SARS-CoV2 main
protease by molecular docking and simulation studies. J. Biomol. Struct. Dyn.
2020, 1–12. doi: 10.1080/07391102.2020.1776157

Halgren, T. A., Murphy, R. B., Friesner, R. A., Beard, H. S., Frye, L. L., Pollard, W.
T., et al. (2004). Glide: a new approach for rapid, accurate docking and scoring.
2. Enrichment factors in database screening. J. Med. Chem. 47, 1750–1759.
doi: 10.1021/jm030644s

Harder, E., Damm, W., Maple, J., Wu, C., Reboul, M., Xiang, J. Y., et al. (2016).
OPLS3: a force field providing broad coverage of drug-like small molecules
and proteins. J. Chem. Theory Comput. 12, 281–296. doi: 10.1021/acs.jctc.5b00864

Heaton, S. M., Borg, N. A., and Dixit, V. M. (2015). Ubiquitin in the activation
and attenuation of innate antiviral immunity. J. Exp. Med. 213, 1–13.
doi: 10.1084/jem.20151531

Huang, Y., Dai, H., and Ke, R. (2019). Principles of effective and robust innate
immune response to viral infections: a multiplex network analysis. Front.
Immunol. 10:1736. doi: 10.3389/fimmu.2019.01736

Hypernet Labs and Galileo (2020). Available online at: https://galileoapp.io/

Jacobson, J. M., Feinman, L., Liebes, L., Ostrow, N., Koslowski, V., Tobia,
A., et al. (2001). Pharmacokinetics, safety, and antiviral effects of
hypericin, a derivative of st. john's wort plant, in patients with chronic
hepatitis C virus infection. Antimicrob. Agents Chemother. 45, 517–524.
doi: 10.1128/AAC.45.2.517-524.2001

Jena, A., Kanungo, N., Nayak, V., Chainy, G. B. N., and Dandapat, J. (2020).
Catechin and curcumin interact with corona (2019-nCoV/SARS-CoV2)
viral S protein and ACE2 of human cell insights from computational
study and implication for intervention. Res. Square [Preprint].
doi: 10.21203/rs.3.rs-22057/v1

Jendele, L., Krivak, R., Skoda, P., Novotny, M., and Hoksza, D. (2019). PrankWeb:
a web server for ligand binding site prediction and visualization. Nucleic Acids
Res. 47, W345–W349. doi: 10.1093/nar/gkz424

Jeong, G. U., Song, H., Yoon, G. Y., Kim, D., and Kwon, Y. C. (2020). Therapeutic
strategies against COVID-19 and structural characterization of SARS-CoV-2: a
review. Front. Microbiol. 11:1723. doi: 10.3389/fmicb.2020.01723

Jiang, X., and Chen, Z. J. (2011). The role of ubiquitylation in immune defence and
pathogen evasion. Nat. Rev. Immunol. 12, 35–48. doi: 10.1038/nri3111

Jorgensen, W. L., Maxwell, D. S., and Tirado-Rives, J. (1996). Development
and testing of the OPLS all-atom force field on conformational energetics
and properties of organic liquids. J. Am. Chem. Soc. 118, 11225–11236.
doi: 10.1021/ja9621760

Jorgensen, W. L., and Tirado-Rives, J. (1988). The OPLS [optimized potentials
for liquid simulations] potential functions for proteins, energy minimizations
for crystals of cyclic peptides and crambin. J. Am. Chem. Soc. 110, 1657–1666.
doi: 10.1021/ja00214a001

Kim, S., Chen, J., Cheng, T., Gindulyte, A., He, J., He, S., et al. (2019). PubChem
2019 update: improved access to chemical data. Nucleic Acids Res. 47, D1102–
D1109. doi: 10.1093/nar/gky1033

Klemm, T., Ebert, G., Calleja, D. J., Allison, C. C., Richardson, L. W., Bernardini,
J. P., et al. (2020). Mechanism and inhibition of the papain-like protease, PL^{pro},
of SARS-CoV-2. EMBO J. 39:e106275. doi: 10.15252/embj.2020106275

Komander, D., and Rape, M. (2012). The ubiquitin code. Annu. Rev. Biochem. 81,
203–229. doi: 10.1146/annurev-biochem-060310-170328

Krupanidhi, S., Abraham Peele, K., Venkateswarulu, T. C., Ayyagari, V.
S., Nazneen Bobby, M., John Babu, D., et al. (2020). Screening of
phytochemical compounds of tinospora cordifolia for their inhibitory activity
on SARS-CoV-2: an in silico study. J. Biomol. Struct. Dyn. 2020, 1–5.
doi: 10.1080/07391102.2020.1787226

Kumari, P., and Kumar, H. (2018). Viral deubiquitinases: role in evasion
of anti-viral innate immunity. Crit. Rev. Microbiol. 44, 304–317.
doi: 10.1080/1040841X.2017.1368999

Lee, H., Lei, H., Santarsiero, B. D., Gatuz, J. L., Cao, S., Rice, A. J., et al.
(2015). Inhibitor recognition specificity of MERS-CoV papain-like protease
may differ from that of SARS-CoV. ACS Chem. Biol 10, 1456–1465.
doi: 10.1021/cb500917m

Li, J., Chai, Q. Y., and Liu, C. H. (2016). The ubiquitin system: a critical regulator
of innate immunity and pathogen–host interactions. Cell. Mol. Immunol. 13,
560–576. doi: 10.1038/cmi.2016.40

Li, S. Y., Chen, C., Zhang, H. Q., Guo, H. Y., Wang, H., Wang, L.,
et al. (2005). Identification of natural compounds with antiviral
activities against SARS-associated coronavirus. Antiviral Res. 67, 18–23.
doi: 10.1016/j.antiviral.2005.02.007

Liang, J., Pitsillou, E., Karagiannis, C., Darmawan, K. K., Ng, K., Hung, A., et al.
(2020). Interaction of the prototypical alpha-ketoamide inhibitor with the
SARS-CoV-2 main protease active site in silico: molecular dynamic simulations
highlight the stability of the ligand-protein complex. Comput. Biol. Chem.
87:107292. doi: 10.1016/j.compbiolchem.2020.107292

Liu, J., Qian, C., and Cao, X. (2016). Post-translational modification control of
innate immunity. Immunity 45, 15–30. doi: 10.1016/j.immuni.2016.06.020

Madhavi Sastry, G., Adzhigirey, M., Day, T., Annabhimoju, R., and Sherman, W.
(2013). Protein and ligand preparation: parameters, protocols, and influence
on virtual screening enrichments. J. Comput. Aided Mol. Des. 27, 221–234.
doi: 10.1007/s10822-013-9644-8

Mani, J. S., Johnson, J. B., Steel, J. C., Broszczak, D. A., Neilsen, P. M., Walsh, K. B., et al. (2020). Natural product-derived phytochemicals as potential agents against coronaviruses: a review. *Virus Res.* 284:197989. doi: 10.1016/j.virusres.2020.197989

McClain, C. B., and Vabret, N. (2020). SARS-CoV-2: the many pros of targeting PLpro. *Signal Transduct Target Ther.* 5:223. doi: 10.1038/s41392-020-00335-z

Mohammadi Pour, P., Fakhri, S., Asgary, S., Farzaei, M. H., and Echeverría, J. (2019). The signaling pathways, and therapeutic targets of antiviral agents: focusing on the antiviral approaches and clinical perspectives of anthocyanins in the management of viral diseases. *Front. Pharmacol.* 10:1207. doi: 10.3389/fphar.2019.01207

Montoya, A., Daza, A., Muñoz, D., Ríos, K., Taylor, V., Cedeño, D., et al. (2015). Development of a novel formulation with hypericin to treat cutaneous leishmaniasis based on photodynamic therapy in *in vitro* and *in vivo* studies. *Antimicrob. Agents Chemother.* 59, 5804–5813. doi: 10.1128/AAC.00545-15

Muhseen, Z. T., Hameed, A. R., Al-Hasani, H. M. H., Tahir ul Qamar, M., and Li, G. (2020). Promising terpenes as SARS-CoV-2 spike receptor-binding domain (RBD) attachment inhibitors to the human ACE2 receptor: integrated computational approach. *J. Mol. Liq.* 320:114493. doi: 10.1016/j.molliq.2020.114493

Napoli, E., Siracusa, L., Ruberto, G., Carrubba, A., Lazzara, S., Speciale, A., et al. (2018). Phytochemical profiles, phototoxic and antioxidant properties of eleven hypericum species – a comparative study. *Phytochemistry* 152, 162–173. doi: 10.1016/j.phytochem.2018.05.003

Nelemans, T., and Kikkert, M. (2019). Viral innate immune evasion and the pathogenesis of emerging RNA virus infections. *Viruses* 11:961. doi: 10.3390/v11100961

Ngwa, W., Kumar, R., Thompson, D., Lyerly, W., Moore, R., Reid, T. E., et al. (2020). Potential of flavonoid-inspired phytomedicines against COVID-19. *Molecules* 25:2707. doi: 10.3390/molecules25112707

Ohtake, F., Tsuchiya, H., Saeki, Y., and Tanaka, K. (2018). K63 ubiquitylation triggers proteasomal degradation by seeding branched ubiquitin chains. *Proc. Natl. Acad. Sci. U.S.A.* 115:E1401. doi: 10.1073/pnas.1716673115

Ojha, P. K., Kar, S., Krishna, J. G., Roy, K., and Leszczynski, J. (2020). Therapeutics for COVID-19: from computation to practices—where, where we are heading to. *Mol. Divers.* doi: 10.1007/s11030-020-10134-x. [Epub ahead of print].

Osipiuk, J., Jedrzejczak, R., Tesar, C., Endres, M., Stols, L., Babnigg, G., et al. (2020). The crystal structure of papain-like protease of SARS CoV-2. *6W9C.* doi: 10.2210/pdb6W9C/pdb

Pan, H., Peto, R., Karim, Q. A., Alejandria, M., Henao-Restrepo, A. M., García, C. H., et al. (2020). Repurposed antiviral drugs for COVID-19 –interim WHO SOLIDARITY trial results. *medRxiv [Preprint].* doi: 10.1101/2020.10.15.20209817

Pan, H. D., Yao, X. J., Wang, W. Y., Lau, H. Y., and Liu, L. (2020). Network pharmacological approach for elucidating the mechanisms of traditional Chinese medicine in treating COVID-19 patients. *Pharmacol. Res.* 159:105043. doi: 10.1016/j.phrs.2020.105043

Pandey, A., Nikam, A. N., Shreya, A. B., Mutalik, S. P., Gopalan, D., Kulkarni, S., et al. (2020). Potential therapeutic targets for combating SARS-CoV-2: drug repurposing, clinical trials and recent advancements. *Life Sci.* 256:117883. doi: 10.1016/j.lfs.2020.117883

Panier, S., and Durocher, D. (2009). Regulatory ubiquitylation in response to DNA double-strand breaks. *DNA Rep.* 8, 436–443. doi: 10.1016/j.dnarep.2009.01.013

Panyod, S., Ho, C. T., and Sheen, L. Y. (2020). Dietary therapy and herbal medicine for COVID-19 prevention: a review and perspective. *J. Tradition. Complement. Med.* 10, 420–427. doi: 10.1016/j.jtcme.2020.05.004

Perng, Y. C., and Lenschow, D. J. (2018). ISG15 in antiviral immunity and beyond. *Nat. Rev. Microbiol.* 16, 423–39. doi: 10.1038/s41579-018-0020-5

Petersen, E., Koopmans, M., Go, U., Hamer, D. H., Petrosillo, N., Castelli, F., et al. (2020). Comparing SARS-CoV-2 with SARS-CoV and influenza pandemics. *Lancet Infect. Dis.* 20, e238–e244. doi: 10.1016/S1473-3099(20)30484-9

Pickart, C. M. (2001). Mechanisms underlying ubiquitination. *Annu. Rev. Biochem.* 70, 503–533. doi: 10.1146/annurev.biochem.70.1.503

Pitsillou, E., Liang, J., Karagiannis, C., Ververis, K., Darmawan, K. K., Ng, K., et al. (2020). Interaction of small molecules with the SARS-CoV-2 main protease *in silico* and *in vitro* validation of potential lead compounds using an enzyme-linked immunosorbent assay. *Comput. Biol. Chem.* 2020:107408. doi: 10.1016/j.compbiolchem.2020.107408

Ratia, K., Kilianski, A., Baez-Santos, Y. M., Baker, S. C., and Mesecar, A. (2014). Structural basis for the ubiquitin-linkage specificity and deISGylating activity of SARS-CoV papain-like protease. *PLoS Pathog.* 10:e1004113. doi: 10.1371/journal.ppat.1004113

Ratia, K., Pegan, S., Takayama, J., Sleeman, K., Coughlin, M., Baliji, S., et al. (2008). A noncovalent class of papain-like protease/deubiquitinase inhibitors blocks SARS virus replication. *Proc. Natl. Acad. Sci. U.S.A.* 105:16119. doi: 10.1073/pnas.0805240105

Rook, A. H., Wood, G. S., Duvic, M., Vonderheid, E. C., Tobia, A., and Cabana, B. (2010). A phase II placebo-controlled study of photodynamic therapy with topical hypericin and visible light irradiation in the treatment of cutaneous T-cell lymphoma and psoriasis. *J. Am. Acad. Dermatol.* 63, 984–990. doi: 10.1016/j.jaad.2010.02.039

Russo, M., Moccia, S., Spagnuolo, C., Tedesco, I., and Russo, G. L. (2020). Roles of flavonoids against coronavirus infection. *Chem. Biol. Interact.* 328:109211. doi: 10.1016/j.cbi.2020.109211

Rut, W., Lv, Z., Zmudzinski, M., Patchett, S., Nayak, D., Snipas, S. J., et al. (2020). Activity profiling and crystal structures of inhibitor-bound SARS-CoV-2 papain-like protease: a framework for anti–COVID-19 drug design. *Sci. Adv.* 6:eabd4596. doi: 10.1126/sciadv.abd4596

Sacco, M., Ma, C., Wang, J., and Chen, Y. (2020). Crystal structure of the native SARS-CoV-2 papain-like protease (PL^{Pro}) with inhibitor GRL0617. *7JRN.* doi: 10.2210/pdb7JRN/pdb

Schrödinger (2020a). *Schrödinger Release 2020-2: Maestro.* New York, NY: Schrödinger, LLC.

Schrödinger (2020b). *Schrödinger Release 2020-2: LigPrep.* New York, NY: Schrödinger, LLC.

Schrödinger (2020c). *Schrödinger Release 2020-2: Glide.* New York, NY: Schrödinger LLC.

Shih, C. M., Wu, C. H., Wu, W. J., Hsiao, Y. M., and Ko, J. L. (2018). Hypericin inhibits hepatitis C virus replication via deacetylation and down-regulation of heme oxygenase-1. *Phytomedicine* 46, 193–198. doi: 10.1016/j.phymed.2017.08.009

Shin, D., Mukherjee, R., Grewe, D., Bojkova, D., Baek, K., Bhattacharya, A., et al. (2020). Papain-like protease regulates SARS-CoV-2 viral spread and innate immunity. *Nature* 587, 657–662. doi: 10.1038/s41586-020-2601-5

Shivakumar, D., Williams, J., Wu, Y., Damm, W., Shelley, J., and Sherman, W. (2010). Prediction of absolute solvation free energies using molecular dynamics free energy perturbation and the OPLS force field. *J. Chem. Theory Comput.* 6, 1509–1519. doi: 10.1021/ct900587b

Sinha, S. K., Prasad, S. K., Islam, M. A., Gurav, S. S., Patil, R. B., AlFaris, N. A., et al. (2020). Identification of bioactive compounds from glycyrrhiza glabra as possible inhibitor of SARS-CoV-2 spike glycoprotein and non-structural protein-15: a pharmacoinformatics study. *J. Biomol. Struct. Dyn.* 2020, 1–15. doi: 10.1080/07391102.2020.1779132

Smith, M., and Smith, J. (2020). Repurposing therapeutics for COVID-19: supercomputer-based docking to the SARS-CoV-2 viral spike protein and viral spike protein-human ACE2 interface. *ChemRxiv [Preprint].* doi: 10.26434/chemrxiv.11871402

Subbaiyan, A., Ravichandran, K., Singh, S., Sankar, M., Thomas, P., Dhama, K., et al. (2020). *in silico* molecular docking analysis of targeting SARS-CoV-2 spike protein and selected herbal constituents. *J. Pure Appl. Microbiol.* 14, 775–788. doi: 10.22207/JPAM.14.SPL1.37

Tahir Ul Qamar, M., Alqahtani, S. M., Alamri, M. A., and Chen, L. L. (2020). Structural basis of SARS-CoV-2 3CL(pro) and anti-COVID-19 drug discovery from medicinal plants. *J Pharm Anal.* 10, 313–319. doi: 10.1016/j.jpha.2020.03.009

Tiwari, R., Latheef, S., Ahmed, I., Iqbal, H., Bule, M., Dhama, K., et al. (2018). Herbal immunomodulators, a remedial panacea for the designing and developing effective drugs and medicines: current scenario and future prospects. *Curr. Drug Metab.* 19, 264–301. doi: 10.2174/1389200219666180129125436

Tripathi, M. K., Singh, P., Sharma, S., Singh, T. P., Ethayathulla, A. S., and Kaur, P. (2020). Identification of bioactive molecule from Withania somnifera (Ashwagandha) as SARS-CoV-2 main protease inhibitor. *J. Biomol. Struct. Dyn.* 2020, 1–14. doi: 10.1080/07391102.2020.1790425

Trott, O., and Olson, A. J. (2010). AutoDock Vina: improving the speed and accuracy of docking with a new scoring function, efficient optimization,

and multithreading. *J. Comput. Chem.* 31, 455–461. doi: 10.1002/jcc.2
1334

Verma, S., Twilley, D., Esmear, T., Oosthuizen, C. B., Reid, A. M., Nel, M., et al.
(2020). Anti-SARS-CoV natural products with the potential to inhibit SARS-
CoV-2 (COVID-19). *Front. Pharmacol.* 11:1514. doi: 10.3389/fphar.2020.56
1334

Wang, Z., Sun, H., Yao, X., Li, D., Xu, L., Li, Y., et al. (2016). Comprehensive
evaluation of ten docking programs on a diverse set of protein–ligand
complexes: the prediction accuracy of sampling power and scoring
power. *Phys. Chem. Chem. Phys.* 18, 12964–12975. doi: 10.1039/C6CP01
555G

World Health Organization (2020). *Coronavirus Disease 2019 (COVID-19):
Situation Report 51.*

Yan, Y., Tao, H., He, J., and Huang, S. Y. (2020). The HDOCK server
for integrated protein–protein docking. *Nat. Protoc.* 15, 1829–1852.
doi: 10.1038/s41596-020-0312-x

Yan, Y., Zhang, D., Zhou, P., Li, B., and Huang, S. Y. (2017). HDOCK: a
web server for protein-protein and protein-DNA/RNA docking based on
a hybrid strategy. *Nucleic Acids Res.* 45, W365–W373. doi: 10.1093/nar/
gkx407

Zhang, R., Zhu, X., Bai, H., and Ning, K. (2019). Network
pharmacology databases for traditional chinese medicine: review
and assessment. *Front. Pharmacol.* 10:123. doi: 10.3389/fphar.2019.
00123

Zhou, Y., Hou, Y., Shen, J., Huang, Y., Martin, W., and Cheng, F. (2020). Network-
based drug repurposing for novel coronavirus 2019-nCoV/SARS-CoV-2. *Cell
Discov.* 6:14. doi: 10.1038/s41421-020-0153-3

Zhou, Z., Zhu, X., Yin, R., Liu, T., Yang, S., Zhou, L., et al. (2020). K63
ubiquitin chains target NLRP3 inflammasome for autophagic degradation
in ox-LDL-stimulated THP-1 macrophages. *Aging* 12, 1747–1759.
doi: 10.18632/aging.102710

Conflict of Interest: Epigenomic Medicine Program (TCK) is supported
financially by McCord Research (Iowa, USA), which has a financial interest in
dietary compounds described in this work. However, there is no conflict of interest
with respect to the inhibition of the SARS-CoV-2 papain-like protease.

The remaining authors declare that the research was conducted in the absence of
any commercial or financial relationships that could be construed as a potential
conflict of interest.